THE EUROPEAN
PHYSICAL JOURNAL C

CrossMark

Study of the excited 1^- charm and charm–strange mesons

Qiang Li[1,a], **Yue Jiang**[1,b], **Tianhong Wang**[1,c], **Han Yuan**[1,d], **Guo-Li Wang**[1,e], **Chao-Hsi Chang**[2,3,f]

[1] Harbin Institute of Technology, Harbin 150001, People's Republic of China
[2] CCAST (World Laboratory), P.O. Box 8730, Beijing 100080, People's Republic of China
[3] Institute of Theoretical Physics, Chinese Academy of Sciences, P.O. Box 2735, Beijing 100080, People's Republic of China

Abstract We give a systematical study on the recently reported excited charm and charm–strange mesons with potential 1^- spin–parity, including the $D_{s1}^*(2700)^+$, $D_{s1}^*(2860)^+$, $D^*(2600)^0$, $D^*(2650)^0$, $D_1^*(2680)^0$ and $D_1^*(2760)^0$. The main strong decay properties are obtained in the framework of Bethe–Salpeter (BS) methods. Our results reveal that the two 1^- charm–strange mesons can be well described by the further 2^3S_1–1^3D_1 mixing scheme with a mixing angle of $(8.7^{+3.9}_{-3.2})°$. The predicted decay ratio $\frac{\mathcal{B}(D^*K)}{\mathcal{B}(D\,K)}$ for $D_{s1}^*(2860)$ is $0.62^{+0.22}_{-0.12}$. $D^*(2600)^0$ can also be explained as the 2^3S_1 predominant state with a mixing angle of $-(7.5^{+4.0}_{-3.3})°$. Considering the mass range, $D^*(2650)^0$ and $D_1^*(2680)^0$ are more likely to be the 2^3S_1 predominant states, although the total widths under the two 2^3S_1 and 1^3D_1 assignments have no great conflict with the current experimental data. The calculated width for the LHCb $D_1^*(2760)^0$ seems to be about $100\,\mathrm{MeV}$ larger than the experimental measurement if taking it as 1^3D_1 or 1^3D_1 dominant state $c\bar{u}$. The comparisons with other calculations and several important decay ratios are also presented. For the identification of these 1^- charm mesons, further experimental information, such as $\frac{\mathcal{B}(D\pi)}{\mathcal{B}(D^*\pi)}$, is necessary.

1 Introduction

Recently lots of natural parity charm and charm–strange mesons have been observed in experiments [1–10], which are summarized in Table 1, where we have combined the statistical, systematic and model errors in quadrature for simplicity.

[a] e-mail: lrhit@protonmail.com

[b] e-mail: jiangure@hit.edu.cn

[c] e-mail: thwang@hit.edu.cn

[d] e-mail: hanyuan@hit.edu.cn

[e] e-mail: gl_wang@hit.edu.cn

[f] e-mail: zhangzx@itp.ac.cn

These new resonances have great importance in improving our knowledge of the radial and orbital charmed excitations. Especially for the spin–parity 1^- charm and charm–strange states, there may exist 2^3S_1–1^3D_1 mixing, which makes the assignments more complicated.

$D_{s1}^*(2700)^+$ was first discovered by Belle collaboration in 2008 [1] in channel $D_{s1}^*(2700)^+ \to D^0K^+$, and then confirmed by BaBar in 2009 [2] and LHCb in 2012 [4]. Furthermore, the BaBar collaboration also obtained two ratios of branching fractions [2],

$$R_K[D_{s1}^*(2700)^+] \equiv \frac{\mathcal{B}[D_{s1}^*(2700)^+ \to D^*K]}{\mathcal{B}[D_{s1}^*(2700)^+ \to DK]}$$
$$= 0.91 \pm 0.13_{\mathrm{stat}} \pm 0.12_{\mathrm{syst}}, \quad (1)$$

$$R_K[D_{sJ}^*(2860)^+] \equiv \frac{\mathcal{B}[D_{sJ}^*(2860)^+ \to D^*K]}{\mathcal{B}[D_{sJ}^*(2860)^+ \to DK]}$$
$$= 1.1 \pm 0.15_{\mathrm{stat}} \pm 0.19_{\mathrm{syst}}, \quad (2)$$

where we have defined the abbreviation R_K for simplicity. $D_{sJ}^*(2860)^+$ were first detected by BaBar together with the $D_{s1}^*(2700)^+$ and then confirmed by LHCb [4]. However, there are about 3σ discrepancies in the total width. This discrepancy was resolved by LHCb's subsequent measurement with the amplitude analysis in 2014 [6], which find that the structure $D_{sJ}^*(2860)^+$ contains both spin-1 and spin-3 components, while a larger width of the former one is preferred. The potential models predict that the masses of 2^3S_1 and 1^3D_1 charm–strange mesons are around 2.73 and 2.90 GeV, respectively [11,12]. The $D_{s1}^*(2700)^+$ and $D_{s1}^*(2860)^+$ are then usually interpreted as the 2^3S_1 and 1^3D_1 charm–strange mesons, respectively. There is much work on the properties of these two resonances. The $D_{s1}^*(2700)^+$ is identified as the 2^3S_1 $c\bar{s}$ in Refs. [13–17], while in Ref. [18] the 1^3D_1 assignments are favored. Almost all the pure $2S$ or $1D$ assignments have difficulty in producing the experimental ratio $R_K[D_{s1}^*(2700)] = 0.91$. In Refs. [15,19–24] the $2S$–$1D$ mixing states of $D_{s1}^*(2700)^+$ and $D_{s1}^*(2860)^+$ are discussed, and we will discuss the mixing scheme in detail

Table 1 Experimental results of the recently discovered excited open charm mesons with natural spin–parity

Resonance	Mass (MeV)	Width (MeV)	J^P	References	Time
$D_{s1}^*(2700)^+$	2708 ± 14	108 ± 36	1^-	Belle [1]	2008
	2710 ± 12	149 ± 52.5		BaBar [2]	2009
	2709.3 ± 4.9	115.8 ± 14.1		LHCb [4]	2012
	2709 ± 4	117 ± 13		PDG [7]	2014
	2699^{+14}_{-7}	127^{+24}_{-19}		BaBar [8]	2015
$D_{sJ}^*(2860)^+$	2862 ± 5.4	48 ± 6.7	Natural	BaBar [2]	2009
	2866.1 ± 6.4	69.9 ± 7.3	Natural	LHCb [4]	2012
	2859 ± 27	159 ± 80	1^-	LHCb [6]	2014
	2860.5 ± 7	53 ± 10	3^-	LHCb [6]	2014
$D^*(2600)^0$	2608.7 ± 3.5	93 ± 14.3	Natural	BaBar [3]	2010
$D^*(2650)^0$	2649.2 ± 4.9	140 ± 25.5	Natural	LHCb [5]	2013
$D_1^*(2680)^0$	2681.1 ± 15.1	186.7 ± 14.6	1^-	LHCb [10]	2016
$D^*(2760)^0$	2763.3 ± 3.3	60.9 ± 6.2	Natural	BaBar [3]	2010
$D_J^*(2760)^0$	2760.1 ± 3.9	74.4 ± 19.4	Natural	LHCb [5]	2013
$D_3^*(2760)^0$	2775.5 ± 7.9	95.3 ± 35.4	3^-	LHCb [10]	2016
$D_1^*(2760)^0$	2781 ± 21.9	177 ± 38.4	1^-	LHCb [9]	2015
$D_J^*(3000)^0$	3008.1 ± 4.0	110.5 ± 11.5	Natural	LHCb [5]	2013
$D_2^*(3000)^0$	3214 ± 56.8	186 ± 81.0	2^+	LHCb [10]	2016
$D^*(2600)^+$	2621.3 ± 5.6	93	Natural	BaBar [3]	2010
$D^*(2760)^+$	2769.7 ± 4.1	60.9	Natural	BaBar [3]	2010
$D_J^*(2760)^+$	2771.7 ± 4.2	66.7 ± 12.4	Natural	LHCb [5]	2013
$D_3^*(2760)^-$	2798 ± 9.9	105 ± 29.8	3^-	LHCb [9]	2015
$D_J^*(3000)^+$	3008.1 (fixed)	110.5 (fixed)	Natural	LHCb [5]	2013

in Sect. 3. Besides the conventional assignments, Ref. [25] argued that the $D_{sJ}^*(2860)^+$ can be explained as $D_1(2420)K$ bound states by using the chiral and heavy quark symmetry.

For the corresponding charm mesons, the Godfrey–Isgur (GI) model [11,12] predicts the 2^3S_1 and 1^3D_1 states $c\bar{u}$ locate in the mass range of about 2.64 and 2.82 GeV, respectively, while the mass of 1^3D_3 state is predicted to be quite close to the 1^3D_1 state. BaBar in 2010 [3] reported two natural parity resonances $D^*(2600)^0$ and $D^*(2760)^0$. Furthermore, they measured the following ratio of the branching fraction:

$$R_{D^+}[D^*(2600)^0] \equiv \frac{\mathcal{B}[D^*(2600)^0 \to D^+\pi^-]}{\mathcal{B}[D^*(2600)^0 \to D^{*+}\pi^-]}$$
$$= 0.32 \pm 0.02_{\text{stat}} \pm 0.09_{\text{syst}}. \quad (3)$$

Again we have introduced the abbreviation R_{D^+} for the sake of simplicity. Later in 2013 LHCb [5] discovered two natural parity charmed particle $D^*(2650)^0$ and $D_J^*(2760)^0$. Then in 2015 LHCb [9] reported the 1^- state $D_1^*(2760)^0$, which has a large width of 177 ± 38 MeV. Very recently, in 2016 by using the amplitude analysis, LHCb collaboration measured a 1^- state $D_1^*(2680)^0$ and a 3^- state $D_3^*(2760)^0$ [10]. The latter one's mass and total width seem consistent with the BaBar $D^*(2760)^0$ and LHCb $D_J^*(2760)^0$. These

experimental data are also summarized in Table 1, where the isospin partners of these neutral charm mesons are also listed in the bottom of Table 1 for comparison. $D^*(2760)^0$, $D_J^*(2760)^0$ and $D_3^*(2760)^0$ can be interpreted as the same particle, namely, the 3^- state $c\bar{u}$, while this interpretation is favored by Refs. [15,26–28]. Then there are still four natural parity resonances, $D^*(2600)^0$, $D^*(2650)^0$, $D_1^*(2680)^0$ and $D_1^*(2760)^0$ in the mass range of 2.6–2.8 GeV. In the tradiional conventions of charm meson spectroscopy, these four resonances should correspond the 2^3S_1 and 1^3D_1 states $c\bar{u}$ or mixtures of them.

These newly observed charm resonances have also been studied with the 2^3S_1, 1^3D_1 assignments or the $2S$–$1D$ mixing scheme in theory by several models, including the nonrelativistic quark model [21,27], the heavy quark effective theory [28,29], the effective Lagrangian approach based on heavy quark chiral symmetry [30], the Eichten–Hill–Quigg (EHQ) decay formula [15,24] and the quark pair creation (QPC) model [23,31–34]. However, the current theoretical calculations for these higher mass charmed mesons cannot be well consistent with the experimental data. We find the calculated ratio $R_{D^+}[D^*(2600)^0]$ for taking it as the 2^3S_1 state is usually greater than the experimental value Eq. (3) [27–30,32], while Ref. [30] argues that no quantum number

assignments for a pure state at mass 2600 MeV is able to reproduce the experimental ratio.

Generally, all the physical mesons have definite J^P spin–parity or J^{PC} for quarkonia. In the relativistic situations, the spin S and orbital angular momentum L are no longer the good quantum numbers, and the physical states are not always located in the definite $^{2S+1}L_J$ states. This situations become obvious in the 1^+ and 1^- mesons, for the 1^+ states we always have to make the $^1P_1$–$^3P_1$ mixing to fit the physical states [35,36], while for the 1^- states the 2^3S_1–1^3D_1 mixing is needed to fit the experimental measurements [37]. So in a more effective and appropriate method to describe the bound state, we should focus on the $J^{P(C)}$, which are the good quantum numbers in any case. In principal, if we use a full relativistic method to solve the eigenstate problem of the bound mesons with definite $J^{P(C)}$, we do not need mixing to fit the data. We have tried this by the BS method in a previous work to study the state $D^*_{s1}(2700)$ [38], based on the BS wave function constructed directly from the quantum number $J^P = 1^-$. The Salpeter wave functions of 1^- states were given, and by solving the full Salpeter equations, we obtain the eigenstates for $c\bar{s}$ and find that all the states include both S and D-wave components. The first state is $1S$ dominant, while D-wave components can be ignored. The second state is $2S$ dominant, which is the first radial excited state. The third state, which is the second radial excited state, is predominant by $1D$ components. But our previous results, including the mass spectra and decays, cannot fit the data very well. The reason is that we also make some approximations. The first is the instantaneous approximation, which assumes the potential is static, since the four-dimensional BS equation with non-static potential is quite difficult. The second is the interaction kernel, where we choose the Coulomb-like plus linear potential. The Coulomb potential comes from the single-gluon exchange, where we only keep the first order of QCD interaction. Also the linear confinement potential is introduced by phenomenological analysis. Since the BS equation is an integral equation, the kernel includes all the ladder diagram contributions but not the cross diagrams and the annihilation diagrams. These approximations have some effects in diagonalizing the mass matrix. So our method is not a full theory and not a full relativistic method, and it cannot exactly fit the experimental measurements. To overcome this discrepancy, we will make a further mixing to fit the physical states. In this study, we will give a continuous study of these 1^- states open charm mesons. We make a further mixing by the second and third radial excited states. Our mixing angle may be smaller than other non-relativistic methods since some relativistic corrections have already been kept in.

In this research, we will calculate the Okubo–Zweig–Iizuka (OZI) allowed strong decays of these potential 1^- charm–strange mesons, $D^*_{s1}(2700)$, $D^*_{s1}(2860)$, and the neutral charm meson $D^*(2600)$, $D^*(2650)$, $D_1^*(2680)$, and $D_1^*(2760)$, where the charge superscripts "+" and "0" are omitted for brevity here and also in the following context. We will focus on the further 2^3S_1–1^3D_1 mixing scheme to discuss the assignments for these resonances, and the BaBar measured ratios Eqs. (1) and (3) are used to restrict the mixing angle. This is studied within the framework of the instantaneous Bethe–Salpeter methods [39,40]. The BS methods have been widely used and showed good performance in the strong decays of heavy mesons [41–44], semi-leptonic and non-leptonic decays [45–47], decay constants calculations and annihilation rates [48–50] etc.

The manuscript is organized as follows: in Sect. 2 we give the theoretical formalisms of the strong decays by BS methods; then in Sect. 3 the numerical results and detailed discusses are present; finally, we give a brief summary and conclusion as regards this work.

2 Theoretical calculations

In this section first we give a brief review on the calculations of transition matrix element and BS methods; then the 1^- state Salpeter wave functions are presented.

2.1 Transition matrix element

The Feynman diagram for strong decays of charmed meson is showed in Fig. 1, where we use the subscripts 1 and 2 to denote the final charmed meson and light meson, respectively. By using the reduction formula, the transition matrix element for the decay $D^*_s \to D^{(*)}K$ can be written as [41]

$$\langle D^{(*)}(P_1)K(P_2)|D^*_s(P)\rangle = \int d^4x\, e^{-iP_2\cdot x}(M_2^2 - P_2^2)$$
$$\times \langle D^{(*)}(P_1)|\Phi_2(x)|D^*_s(P)\rangle, \quad (4)$$

where P, P_1 and P_2 denote the momenta of the initial state D^*_s, final charmed meson $D^{(*)}$ and the final light meson K, respectively (see Fig. 1); M_2 is the mass of the final light meson. $\Phi_2(x)$ is used to describe the light scalar meson field. The partially conserved axial current (PCAC) relation reads

$$\Phi_2(x) = \frac{1}{M_2^2 F_2}\partial_\mu(\bar{s}\Gamma^\mu q), \quad (5)$$

where F_2 is the decay constant of the light scalar meson; $q = u$ or d corresponds to the K^+ and K^0, respectively; the abbreviation $\Gamma^\mu = \gamma^\mu\gamma^5$ is used. Inserting the PCAC relation into Eq. (4), with the low energy theorem, Eq. (4) can be expressed as

$$\langle D^{(*)}(P_1)K(P_2)|D_s^*(P)\rangle$$
$$= (2\pi)^4\delta^4(P - P_1 - P_2)$$
$$\times \frac{-iP_2^\mu}{F_2}\langle D^{(*)}(P_1)|\bar{s}\Gamma_\mu q|D_s^*(P)\rangle. \tag{6}$$

Then the decay amplitude $\mathcal{M}$ can be described by

$$\mathcal{M} = \frac{P_2^\mu}{F_2}\langle D^{(*)}(P_1)|\bar{s}\Gamma_\mu q|D_s^*(P)\rangle, \tag{7}$$

where the transition matrix element $\langle D^{(*)}(P_1)|\bar{s}\Gamma_\mu q|D_s^*(P)\rangle$ can be calculated by the Salpeter method and will be derived in next subsection. The decay width Γ is then expressed by

$$\Gamma = \frac{1}{8\pi}\langle|\mathcal{M}|^2\rangle\frac{|\vec{P}_1|}{M^2}, \tag{8}$$

where $|\vec{P}_1| = \frac{1}{2M}\sqrt{\lambda(M, M_1, M_2)}$ and the Källén function $\lambda(a, b, c) = (a^2 + b^2 + c^2 - 2ab - 2bc - 2ac)$ is used; $\langle|\mathcal{M}|^2\rangle$ stands for the average over initial spins and sum over final spins.

When the light meson is η, η–η' mixing should be considered. In this work we use the following mixing conventions:

$$\begin{bmatrix} \eta \\ \eta' \end{bmatrix} = \begin{bmatrix} \cos\theta_\eta & \sin\theta_\eta \\ -\sin\theta_\eta & \cos\theta_\eta \end{bmatrix}\begin{bmatrix} \eta_8 \\ \eta_1 \end{bmatrix}. \tag{9}$$

η_8 and η_1 are the SU(3) octet and singlet states, respectively. We use the mixing angle $\theta_\eta = 19°$. To include this mixing effect, the PCAC relation reads

$$\Phi_\eta(x) = \cos\theta_\eta\Phi_{\eta_8}(x) + \sin\theta_\eta\Phi_{\eta_1}(x)$$
$$= \frac{\cos\theta_\eta}{M_{\eta_8}^2 f_{\eta_8}}\partial_\mu\left(\frac{\bar{u}\Gamma^\mu u + \bar{d}\Gamma^\mu d - 2\bar{s}\Gamma^\mu s}{\sqrt{6}}\right)$$
$$+ \frac{\sin\theta_\eta}{M_{\eta_1}^2 f_{\eta_1}}\partial_\mu\left(\frac{\bar{u}\Gamma^\mu u + \bar{d}\Gamma^\mu d + \bar{s}\Gamma^\mu s}{\sqrt{3}}\right)$$
$$= \left[\frac{-2\cos\theta_\eta}{\sqrt{6}M_{\eta_8}^2 f_{\eta_8}} + \frac{\sin\theta_\eta}{\sqrt{3}M_{\eta_0}^2 f_{\eta_0}}\right]\partial_\mu(\bar{s}\Gamma^\mu s) \tag{10}$$

where in the last step we have only kept the $\bar{s}\Gamma^\mu s$ part, since the others have no contribution here; f_{η_8} and f_{η_1} are the corresponding decay constants of η_8 and η_1, respectively.

When the π^0 is involved in the final states, the PCAC relation reads

$$\Phi_{\pi^0}(x) = \frac{1}{M_{\pi^0}^2 f_\pi}\partial_\mu\left(\frac{\bar{u}\Gamma^\mu u - \bar{d}\Gamma^\mu d}{\sqrt{2}}\right)$$
$$= \frac{1}{\sqrt{2}M_{\pi^0}^2 f_\pi}\partial_\mu(\bar{u}\Gamma^\mu u) \tag{11}$$

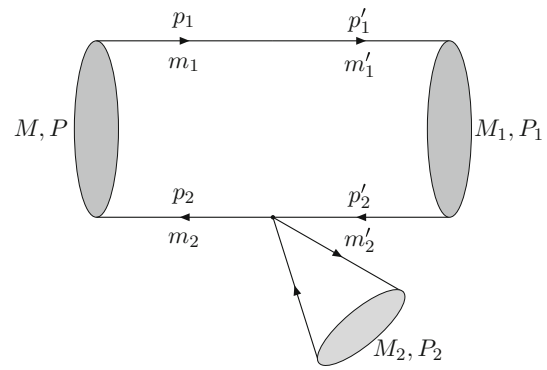Again we have only kept the contributory part.

Fig. 1 Feynman diagram for two body strong decay of $D_{(s)}^*$. $m_1 = m_1' = m_c$, is the constituent mass of the c quark. M_2 and P_2 denote the mass and momentum of the final light meson, respectively

2.2 Transition matrix element with Salpeter wave function

In this subsection we briefly review the BS methods. The BS equation is a four-dimensional integral equation, which reads in momentum space [39]

$$(\not{p}_1 - m_1)\Psi(q)(\not{p}_2 + m_2) = i\int\frac{d^4k}{(2\pi)^4}V(q - k)\Psi(k), \tag{12}$$

where $\Psi(q)$ is the four-dimensional BS wave function; $V(q - k)$ stands for the BS interaction kernel; p_1 and p_2 are the quark and anti-quark momenta, respectively, while m_1 and m_2 are the corresponding masses (see Fig. 1). It is more convenient to express the p_1 and p_2 with the total momentum P and the inner relative momentum q as

$$p_1 = \alpha_1 P + q, \quad p_2 = \alpha_2 P - q. \tag{13}$$

α_i ($i = 1, 2$) is defined as $\alpha_i \equiv \frac{m_i}{m_1 + m_2}$. The Salpeter wave function $\varphi(q_\perp)$ is related to the BS wave function $\Psi(q)$ by the following definition:

$$\varphi(q_\perp) \equiv i\int\frac{dq_P}{2\pi}\Psi(q),$$
$$\eta(q_\perp) \equiv \int\frac{d^3k_\perp}{(2\pi)^3}\varphi(k_\perp)V(|q_\perp - k_\perp|), \tag{14}$$

where $q_P = \frac{P \cdot q}{M}$ and $q_\perp = q - \frac{P}{M}q_P$, in the rest frame of the initial meson they correspond to q^0 and $\vec{q}$, respectively; the three-dimensional integration $\eta(q_\perp)$ can be understood as the BS vertex for bound states; $V(|q_\perp - k_\perp|)$ denotes the instantaneous interaction kernel, namely, the inner interaction are assumed to be a static potential. As usual, in this work, the specific interaction kernel $V(r)$ we use is the Coulomb-like potential plus the unquenched scalar confinement one [48],

$$V(r) = V_s(r) + V_0 + \gamma_0 \otimes \gamma^0 V_v(r)$$
$$= \frac{\lambda}{\alpha}(1 - e^{-\alpha r}) + V_0 - \gamma_0 \otimes \gamma^0 \frac{4}{3}\frac{\alpha_s}{r} e^{-\alpha r}, \quad (15)$$

where λ is the string constant, $\alpha_s(r)$ is the running strong coupling constant, and V_0 is a free constant fixed by fitting the data. By Fourier transformation, the potential $V(\vec{q}\,)$ in momentum space reads

$$V(\vec{q}\,) = -\left(\frac{\lambda}{\alpha} + V_0\right)(2\pi)^3 \delta^3(\vec{q}\,) + (2\pi)^3 \frac{\lambda}{\pi^2}\frac{1}{(\vec{q}\,^2 + \alpha^2)^2}$$
$$- \gamma_0 \otimes \gamma^0 (2\pi)^3 \frac{2}{3\pi^2}\frac{\alpha_s(\vec{q}\,)}{(\vec{q}\,^2 + \alpha^2)}, \quad (16)$$

where the running coupling constant $\alpha_s(\vec{q}\,) = \frac{12\pi}{27}\frac{1}{\log(a + \vec{q}\,^2/\Lambda_{QCD}^2)}$. It is clear to see that here we did not include the spin structure in the interaction kernel $V(\vec{q}\,)$. In fact, the effects from the spin and orbital angular momentum are incorporated in the construction of wave functions, which are discussed more detailed in the next subsection on the Salpeter wave functions. And also in the Coulomb vector potential, we have only kept the temporal component and omitted the spatial components, which are suppressed by a factor of $1/c$ for the heavy–light systems in the Coulomb gauge, as stated in Ref. [51]. On the other hand, a full vector $\gamma^\mu \otimes \gamma_\mu$ interaction kernel would also cause the calculations to be much more complicated. So, in a preliminary study, we only keep the time component of the Coulomb vector potential.

Then under the instantaneous approximation, the BS equation (12) can be written as

$$\Psi(q) = S(p_1)\eta(q_\perp)S(-p_2). \quad (17)$$

$S(p_1)$ and $S(-p_2)$ are the propagators for the quark and antiquark, respectively, and they can be decomposed as

$$S(+p_1) = \frac{i\Lambda_1^+}{q_P + \alpha_1 M - \omega_1 + i\epsilon} + \frac{i\Lambda_1^-}{q_P + \alpha_1 M + \omega_1 - i\epsilon},$$
$$S(-p_2) = \frac{i\Lambda_2^+}{q_P - \alpha_2 M + \omega_2 - i\epsilon} + \frac{i\Lambda_2^-}{q_P + \alpha_2 M - \omega_2 + i\epsilon}, \quad (18)$$

where $\omega_i = \sqrt{m_i^2 - q_\perp^2}$ $(i = 1, 2)$. $\Lambda_i^\pm(q_\perp)$ $(i = 1, 2)$ are the projection operators, which have the following forms:

$$\Lambda_i^\pm(q_\perp) = \frac{1}{2\omega_i}\left[\frac{\slashed{P}}{M}\omega_i \pm (-1)^{i+1}(m_i + \slashed{q}_\perp)\right]. \quad (19)$$

It can easily be checked that the projection operators satisfy the following relations:

$$\Lambda_i^+(q_\perp) + \Lambda_i^-(q_\perp) = \frac{\slashed{P}}{M},$$
$$\Lambda_i^\pm(q_\perp)\frac{\slashed{P}}{M}\Lambda_i^\pm(q_\perp) = \Lambda_i^\pm(q_\perp),$$
$$\Lambda_i^\pm(q_\perp)\frac{\slashed{P}}{M}\Lambda_i^\mp(q_\perp) = 0. \quad (20)$$

Since the BS kernel is assumed to be instantaneous, we can perform a contour integration over q_P on both sides of

Eq. (17), then we obtain the Salpeter equation:

$$\varphi(q_\perp) = \frac{\Lambda_1^+(q_\perp)\eta(q_\perp)\Lambda_2^+(q_\perp)}{(M - \omega_1 - \omega_2)}$$
$$- \frac{\Lambda_1^-(q_\perp)\eta(q_\perp)\Lambda_2^-(q_\perp)}{(M + \omega_1 + \omega_2)}. \quad (21)$$

To make a further simplification, we introduce four new wave functions $\varphi^{\pm\pm}(q_\perp)$ with the definitions

$$\varphi^{\pm\pm}(q_\perp) = \Lambda_i^\pm(q_\perp)\frac{\slashed{P}}{M}\varphi(q_\perp)\frac{\slashed{P}}{M}\Lambda_i^\pm(q_\perp), \quad (22)$$

where φ^{++} is then called the positive Salpeter wave function, while φ^{--} is called the negative Salpeter wave function.

Then with the help of Eq. (20), the Salpeter equation (21) can be further expressed as the following four coupled equations [40]:

$$\varphi^{+-}(q_\perp) = \varphi^{-+}(q_\perp) = 0, \quad (23)$$
$$(M - \omega_1 - \omega_2)\varphi^{++}(q_\perp) = +\Lambda_1^+(q_\perp)\eta(q_\perp)\Lambda_2^+(q_\perp), \quad (24)$$
$$(M + \omega_1 + \omega_2)\varphi^{--}(q_\perp) = -\Lambda_1^-(q_\perp)\eta(q_\perp)\Lambda_2^-(q_\perp). \quad (25)$$

From the above equations, we can see that in the weak binding condition, namely, $M \sim (\omega_1 + \omega_2)$, φ^{--} is much smaller compared with φ^{++} and can be ignored in the calculations. However, these four equations play equivalent roles in solving the eigenstate problem. The normalization condition for the Salpeter wave function reads

$$\int \frac{d^3 q_\perp}{(2\pi)^3}\left[\overline{\varphi}^{++}\frac{\slashed{P}}{M}\varphi^{++}\frac{\slashed{P}}{M} - \overline{\varphi}^{--}\frac{\slashed{P}}{M}\varphi^{--}\frac{\slashed{P}}{M}\right] = 2M. \quad (26)$$

According to Mandelstam formalism [52], the transition matrix element $\langle D^{(*)}(P_1)|\bar{s}\Gamma_\mu q|D_s^*(P)\rangle$ can be expressed as

$$\langle D^{(*)}(P_1)|\bar{s}\Gamma^\mu q|D_s^*(P)\rangle$$
$$\simeq \int \frac{d^3\vec{q}}{(2\pi)^3}\text{Tr}\left[\bar{\varphi}_{P_1}'^{++}(|\vec{q}\,'|)\frac{\slashed{P}}{M}\varphi_P^{++}(|\vec{q}\,|)\Gamma^\mu\right], \quad (27)$$

where $\bar{\varphi}_{P_1}'^{++}$ is defined as $\gamma^0(\varphi_{P_1}'^{++})^\dagger\gamma^0$, and $\varphi_{P_1}'^{++}$ is the positive Salpeter wave function of the final state; $\vec{q}\,' = \vec{q} - \frac{m_1'}{m_1' + m_2'}\vec{P}_1$; m_1' and m_2' are the constituent quark and antiquark masses in the final charmed meson (see Fig. 1). To achieve a final result, we still need to know the specific form of the corresponding Salpeter wave functions.

2.3 Relativistic Salpeter wave function

The Salpeter wave functions involved in these calculations include the 0^-, 1^- and 1^+ states, which correspond to the $^1S_0$, $^3S_1(^3D_1)$ and $^1P_1(^3P_1)$ states within the non-relativistic

models. The Salpeter wave function of 0^- state can be found in Ref. [53]. Here we only give the 1^- state Salpeter wave function. The $^3S_1$ and $^3D_1$ states share the same spin–parity $J^P = 1^-$. We rewrite the Salpeter wave function for the 1^- states [48] thus:

$$
\begin{aligned}
&\varphi(1^-) \\
&= \frac{q_\perp \cdot \xi}{|\vec{q}\,|}\left(f_1 + f_2\frac{\slashed{P}}{M} + f_3\frac{\slashed{q}_\perp}{|\vec{q}\,|} + f_4\frac{\slashed{P}\slashed{q}_\perp}{M|\vec{q}\,|}\right) \\
&\quad + i\frac{\epsilon_{\mu P q_\perp \xi}}{M|\vec{q}\,|}\gamma^\mu \\
&\quad \times \left(f_5\frac{\slashed{P}\slashed{q}_\perp}{M|\vec{q}\,|} + f_6\frac{\slashed{q}_\perp}{|\vec{q}\,|} + f_7\frac{\slashed{P}}{M} + f_8\right)\gamma^5,
\end{aligned}
\tag{28}
$$

where f_i $(i = 1, 2, \ldots, 8)$ are the radial wave functions; $\epsilon_{\mu P q_\perp \xi} = \epsilon_{\mu\nu\alpha\beta}P^\nu q_\perp^\alpha \xi^\beta$ and $\epsilon_{\mu\nu\alpha\beta}$ is the totally antisymmetric Levi-Civita tensor; ξ denotes the polarization vector for initial state and fulfills $P \cdot \xi = 0$, $\sum \xi_\mu^{(r)}\xi_\nu^{(r)} = \frac{P_\mu P_\nu}{M^2} - g_{\mu\nu}$. By using the Salpeter equations (23), we obtain the following four constraint conditions:

$$
\begin{aligned}
f_1 &= -\frac{|\vec{q}\,|(\omega_1 + \omega_2)}{m_1\omega_2 + m_2\omega_1}f_3, \quad f_7 = \frac{|\vec{q}\,|(\omega_1 - \omega_2)}{m_1\omega_2 + m_2\omega_1}f_5, \\
f_2 &= -\frac{|\vec{q}\,|(\omega_1 - \omega_2)}{m_1\omega_2 + m_2\omega_1}f_4, \quad f_8 = \frac{|\vec{q}\,|(\omega_1 + \omega_2)}{m_1\omega_2 + m_2\omega_1}f_6,
\end{aligned}
\tag{29}
$$

which leave us with four independent wave functions f_3, f_4, f_5 and f_6, only depending on $|\vec{q}\,|$ directly. ω_i is defined as $\sqrt{m_i^2 + \vec{q}^{\,2}}$ $(i = 1, 2)$. It can be easily checked that, with the above Salpeter wave function, every item in Eq. (28) has the same quantum number, $J^P = 1^-$, which is directly related to the quantum number $^{2S+1}L_J$ of the bound states and contain the $^3S_1$ and $^1D_1$ information naturally. Hence the information from the spin structures is incorporated in the spatial parts of the Salpeter wave function. Notice that this wave function form and constraint conditions for 1^- state are not exactly the same as in Ref. [48]; however, it can be proved that the two forms are totally equivalent.

According to the definitions of Eq. (22), the positive Salpeter wave function φ^{++} for 1^- state is then expressed as

$$
\begin{aligned}
\varphi^{++}(1^-) &= \frac{q_\perp \cdot \xi}{|\vec{q}\,|}\left(A_1 + A_2\frac{\slashed{P}}{M} + A_3\frac{\slashed{q}_\perp}{|\vec{q}\,|} + A_4\frac{\slashed{P}\slashed{q}_\perp}{M|\vec{q}\,|}\right) \\
&\quad + i\frac{\epsilon_{\mu P q_\perp \xi}}{M|\vec{q}\,|}\gamma^\mu\left(A_5 + A_6\frac{\slashed{P}}{M} + A_7\frac{\slashed{q}_\perp}{|\vec{q}\,|} + A_8\frac{\slashed{P}\slashed{q}_\perp}{M|\vec{q}\,|}\right)\gamma^5.
\end{aligned}
\tag{30}
$$

And the corresponding coefficients A_i are

$$
\begin{aligned}
A_1 &= \frac{-q(\omega_1 + \omega_2)}{(m_1\omega_2 + m_2\omega_1)}A_3, \quad A_5 = \frac{q(\omega_1 + \omega_2)}{m_1\omega_2 + m_2\omega_1}A_7, \\
A_2 &= \frac{-q(\omega_1 - \omega_2)}{(m_1\omega_2 + m_2\omega_1)}A_4, \quad A_6 = \frac{q(\omega_1 - \omega_2)}{m_1\omega_2 + m_2\omega_1}A_8, \\
A_3 &= \frac{1}{2}\left(f_3 + \frac{m_1 + m_2}{\omega_1 + \omega_2}f_4\right), \quad A_7 = \frac{1}{2}\left(f_6 - \frac{m_1 + m_2}{\omega_1 + \omega_2}f_5\right), \\
A_4 &= \frac{1}{2}\left(f_4 + \frac{\omega_1 + \omega_2}{m_1 + m_2}f_3\right), \quad A_8 = \frac{1}{2}\left(f_5 - \frac{\omega_1 + \omega_2}{m_1 + m_2}f_6\right).
\end{aligned}
\tag{31}
$$

The negative Salpeter wave function φ^{--} can be obtained similarly or by $\varphi^{--} = \varphi - \varphi^{++}$. Then inserting the expressions of φ^{++} and φ^{--} into the coupled Salpeter equations (24) and (25), we obtain the radial eigenvalue equations, which can be solved numerically. The normalization condition for the 1^- state Salpeter wave functions now becomes

$$
\int \frac{\mathrm{d}^3\vec{q}}{(2\pi)^3}\frac{8\omega_1\omega_2}{3M(m_1\omega_2 + m_2\omega_1)}(f_3 f_4 - 2f_5 f_6) = 1. \tag{32}
$$

The interested reader can find a more detailed procedure for solving the full Salpeter equations in our previous work [46, 53–55].

By solving the Salpeter equations, finally we obtain these eight radial wave functions numerically, which are showed in Fig. 2. Figure 2a shows the eight radial wave functions of the first radial excited state, and Fig. 2b shows the radial wave functions of the second radial excited state. From the two diagrams, also considering that in Eq. (28), the direction of momentum $\slashed{q}_\perp$ has a contribution to the S or D wave [56], we can conclude that both the first and the second radial excited states have S and D wave components, while the first radial excited state is 2^3S_1 predominant and the second radial excited state is 1^3D_1 dominant state, as has been stated in Ref. [57].

Since the decay final states include the 1^+ meson, we show our treatment of their wave functions. Generally, the bound state mesons consisting of unequal masses of quark and antiquark do not have a definite charge conjugation parity. So the physical 1^+ states D_1 and D_1' can be considered as admixtures of 1^{++} ($^3P_1$) and 1^{+-} ($^1P_1$) states. Here we will follow the mixing conventions in Refs. [58,59], where the mixing form for the 1^+ states is defined by the mixing angle α_{1P}:

$$
\begin{bmatrix} |D_1\rangle \\ |D_1'\rangle \end{bmatrix} = \begin{bmatrix} \cos\alpha_{1P} & \sin\alpha_{1P} \\ -\sin\alpha_{1P} & \cos\alpha_{1P} \end{bmatrix}\begin{bmatrix} |1^{+-}\rangle \\ |1^{++}\rangle \end{bmatrix}. \tag{33}
$$

The heavy quark effective theory predicts that, in the limit $m_Q \to \infty$, the mixing angle for 1^+ states are expressed as $\alpha_{1P} = \arctan\sqrt{1/2} = 35.3°$. This result will be used in the strong decay calculations when $D_1^{(\prime)}$ mesons are involved in the final states. The Salpeter wave functions for the 1^{+-} and 1^{++} states can be found in Ref. [60].

Having these numerical Salpeter wave functions, we can calculate the three-dimensional integral of the transition matrix element $\langle D^{(*)}(P_1)|\bar{s}\Gamma^\mu q|D_s^*(P)\rangle$ in Eq. (27). The detailed information on performing this integral can be found in our previous work [43,47].

3 Numerical results and discussions

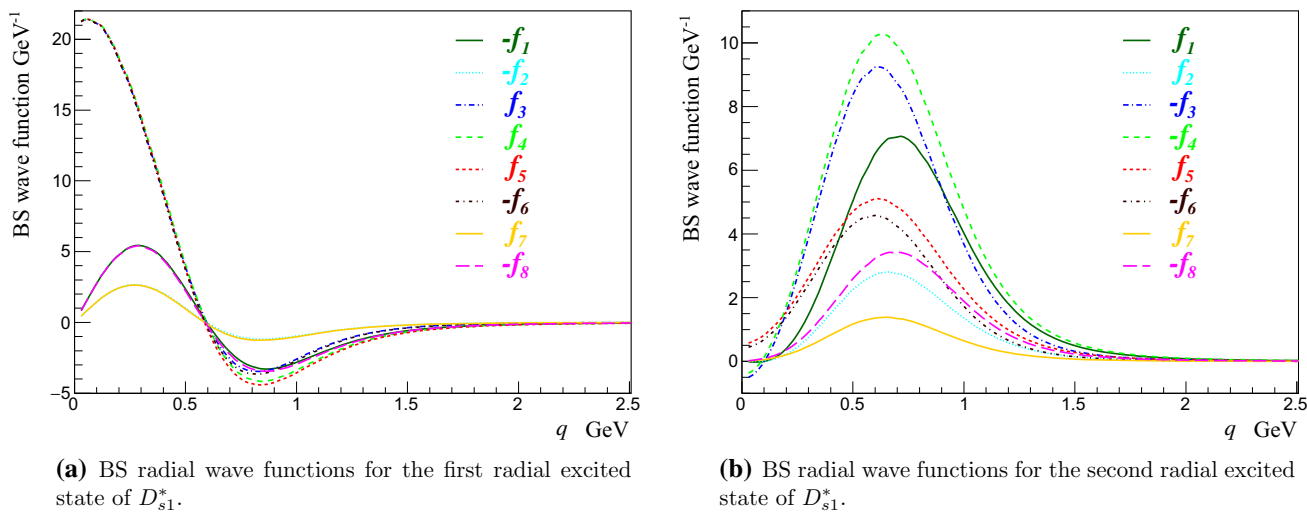First we specify the corresponding parameters used in this work. The decay constants we used are $f_\pi = 130.4$ MeV,

(a) BS radial wave functions for the first radial excited state of D_{s1}^*.

(b) BS radial wave functions for the second radial excited state of D_{s1}^*.

Fig. 2 BS wave function for 1^- radial excited states of D_{s1}^* mesons

$f_K = 156$ MeV [7], $f_{\eta_8} = 1.26 f_\pi$ and $f_{\eta_1} = 1.07 f_\pi$. The mixing angle θ between η–η' we choose is $\theta_\eta = 19°$ with the mixing convention in Eq. (9). The other involved parameters are from PDG data [7] unless otherwise specified. The constituent quark masses and other parameters to characterize the model are

$$a = e = 2.7183, \quad \alpha = 0.060 \text{ GeV}, \quad \lambda = 0.210 \text{ GeV}^2$$
$$\Lambda_{\text{QCD}} = 0.270 \text{ GeV}, \quad m_u = 0.305 \text{ GeV}, \quad m_d = 0.311 \text{ GeV},$$
$$m_s = 0.500 \text{ GeV}, \quad m_c = 1.620 \text{ GeV}, \quad m_b = 4.960 \text{ GeV},$$

which are determined by fitting the mass spectra to the available experimental data [26,61–66]. This set of parameters has been widely used since 2010 in the strong decays of heavy mesons [42–44], semi-leptonic and non-leptonic decays [45–47], and annihilation rates [50] etc. Good performance and consistence with experiments are achieved.

The free parameter V_0 is fixed by fitting the mass eigenvalue to the experimental value. We get V_0 is 0.14 GeV for 1^- charm–strange mesons, while V_0 ranges in $-(0.10$–$0.54)$ GeV when taking $D^*(2600)$, $D^*(2650)$, $D_1^*(2680)$ or $D^*(2760)_1$ as the 2^3S_1 state $c\bar{u}$.

3.1 1^- charm–strange mesons

$D_{s1}^*(2700)$ and $D_{s1}^*(2860)$ share the spin–parity $J^P = 1^-$ determined by experiments. In the first place, we take them as the pure first and second radial excited states, which are dominant by 2^3S_1 and 1^3D_1, respectively. So in this work we still label the first radial excited state as 2^3S_1 and the second excited state by 1^3D_1. The calculated main strong decays properties are listed in Table 2.

From Table 2 we can see that, for $D_{s1}^*(2700)$, neither the 2^3S_1 nor the 1^3D_1 assignment can produce the exper-

Table 2 Decay widths of $D_{s1}^*(2710)$ and $D_{s1}^*(2860)$ as the 2^3S_1 and 1^3D_1 dominant $c\bar{s}$ states in MeV

Mode	2^3S_1		1^3D_1	
	$D_{s1}^*(2700)$	$D_{s1}^*(2860)$	$D_{s1}^*(2700)$	$D_{s1}^*(2860)$
$D^{*0}K^+$	27.5	50.0	6.4	13.0
$D^0 K^+$	17.8	20.8	28.1	38.4
$D^{*+}K^0$	26.6	49.8	6.1	12.7
$D^+ K^0$	17.8	21.3	7.5	38.4
$D_s^{*+}\eta$	0.9	7.6	0.1	1.3
$D_s^+\eta$	2.8	6.0	3.1	7.2
Total	93.4	155.5	51.3	111
$\frac{\mathcal{B}(D^*K)}{\mathcal{B}(DK)}$	1.52	2.37	0.35	0.33

imental ratio $R_K[D_{s1}^*(2700)] = 0.91$, though the 2^3S_1 and 1^3D_1 assignments to $D_{s1}^*(2700)$ and $D_{s1}^*(2860)$, respectively, are roughly consistent with the experimental measurements. Also notice that the total width is only the half of experimental value when taking $D_{s1}^*(2700)$ as the 1^3D_1 state. So these assignments cannot produce experimental data. One also notes that the predicted total decay widths in this paper are larger than our previous calculation [38]; the reason is that we have chosen different $D_{s1}^*(2700)$ mass as input, besides the difference of phase space, and the node structure of the $2S$ state also has a sensitive effect due to the variance of phase space.

Then we introduce the further 2^3S_1–1^3D_1 mixing scheme in the 1^- charm–strange system. The mixing form we used is defined by

$$\begin{bmatrix} |D_{sa}^*\rangle \\ |D_{sb}^*\rangle \end{bmatrix} = \begin{bmatrix} \cos\theta_s & \sin\theta_s \\ -\sin\theta_s & \cos\theta_s \end{bmatrix} \begin{bmatrix} |2^3S_1\rangle \\ |1^3D_1\rangle \end{bmatrix}, \tag{34}$$

and the mixing states D_{sa}^* and D_{sb}^* correspond to $D_{s1}^*(2700)$ and $D_{s1}^*(2860)$, respectively. To get the experimental branching ratio $R_K[D_{s1}^*(2700)] = 0.91_{+0.18}^{-0.18}$, we obtain the mixing angle $\theta_s = (8.7_{-3.2}^{+3.9})°$. Also the relations between original masses and physical masses are determined by the following equation [45,67]:

$$\begin{bmatrix} m_{2S}^2 \\ m_{1D}^2 \end{bmatrix} = \begin{bmatrix} c^2 & s^2 \\ s^2 & c^2 \end{bmatrix} \begin{bmatrix} m_{D_{s1}^*(2700)}^2 \\ m_{D_{s1}^*(2860)}^2 \end{bmatrix}, \qquad (35)$$

where $c = \cos\theta_s$ and $s = \sin\theta_s$. We achieve $m_{2S} = 2.714_{-0.003}^{+0.003}$ and $m_{1D} = 2.857_{+0.002}^{-0.004}$ GeV, respectively. The errors in experimental ratio $R_K[D_{s1}^*(2700)]$ are combined in quadrature for simplicity. The uncertainties in our mixing angle θ_s and other obtained results are induced by varying the experimental ratio $R_K[D_{s1}^*(2700)]$ in the 1σ range.

The decay properties with $2S$–$1D$ mixing are listed in Table 3. The total width for $D_{s1}^*(2700)$ is about 100.8 MeV, which agrees well with the experimental measurement $\Gamma = 117 \pm 13$ MeV [7]. Our results are also consistent with that in Ref. [23], where the mixing angle is about $6.8°$–$11.2°$ and the calculated $\Gamma[D_{s1}^*(2700)]$ is about 100 MeV. With the obtained mixing angle, the total width for $D_{s1}^*(2860)$ we obtain is 108.8 MeV, which is also comparable with the LHCb result $\Gamma[D_s^*(2860)] = 159 \pm 80.3$ MeV, but less than the result $\sim$300 MeV in Ref. [23]. Furthermore, the predicted ratio $R_K[D_{s1}^*(2860)] = 0.62$, which is also consistent with the result 0.6–0.8 in Refs. [17,23,24] and could be used to test this 2^3S_1–1^3D_1 mixing scheme in the future measurements. The comparisons of our results with other predictions can be found in Table 4.

If we do not restrict the mass of the 2^3S_1 state to be less than that of the 1^3D_1 state, we can obtain another large mixing angle, $\theta_s \simeq -77°$, which could also reproduce the experiment ratio $R_K[D_{s1}^*(2710)] = 0.91$. With this mixing angle, we find that the masses before mixing are $m_{2S} = 2.852_{-0.002}^{+0.003}$

Table 3 Decay widths in MeV for $D_{s1}^*(2700)$ and $D_{s1}^*(2860)$ under the further 2^3S_1–1^3D_1 mixing. The mixing angle θ_s is in units of degrees

θ_s	$8.7_{-3.2}^{+3.9}$		$-(76.9_{-1.8}^{+2.2})$	
Mode	$D_{s1}^{*+}(2700)$	$D_{s1}^{*+}(2860)$	$D_{s1}^{*+}(2700)$	$D_{s1}^{*+}(2860)$
$D^{*0}K^+$	$23.3_{+1.5}^{-2.1}$	$19.6_{-2.5}^{+3.2}$	$14.9_{+1.3}^{-1.5}$	$36.1_{-2.1}^{+2.7}$
D^0K^+	$25.2_{-2.8}^{+3.5}$	$31.2_{+2.7}^{-3.6}$	$16.2_{-1.4}^{+1.9}$	$32.7_{+1.6}^{-1.8}$
$D^{*+}K^0$	$22.5_{+1.5}^{-1.9}$	$19.3_{-2.5}^{+3.2}$	$14.3_{+1.3}^{-1.5}$	$36.1_{-2.1}^{+2.6}$
D^+K^0	$25.2_{-2.8}^{+3.3}$	$31.1_{+2.8}^{-3.6}$	$15.9_{-1.5}^{+1.8}$	$33.3_{+1.6}^{-1.8}$
$D_s^{*+}\eta$	$0.8_{+0.0}^{-0.1}$	$2.1_{-0.3}^{+0.4}$	$0.4_{+0.0}^{-0.1}$	$5.7_{-0.2}^{+0.4}$
$D_s^+\eta$	$3.8_{-0.4}^{+0.4}$	$5.5_{-0.7}^{-0.7}$	$1.6_{-0.2}^{+0.2}$	$8.6_{+0.4}^{-0.3}$
Total	$100.8_{-3.0}^{+3.1}$	$108.8_{+0.8}^{-1.1}$	$63.3_{-0.5}^{+0.8}$	$152.3_{-0.8}^{+1.8}$
$\frac{\mathcal{B}(D^*K)}{\mathcal{B}(DK)}$	$0.91_{+0.18}^{-0.18}$	$0.62_{-0.12}^{+0.22}$	$0.91_{+0.18}^{-0.18}$	$1.09_{-0.11}^{+0.15}$

and $m_{1D} = 2.718_{+0.002}^{-0.002}$ GeV, respectively. The strong decay properties are also listed in Table 3. In such a case, $\Gamma[D_{s1}^*(2700)]$ is $\sim$63 MeV, which is about the half of the experimental value; the total width for its orthogonal partner $D_{s1}^*(2860)$ is about 150 MeV; the ratio $R_K[D_{s1}^*(2860)]$ is 1.09. References [19–21] also obtained a large mixing angle $-(57$–$77)°$. We notice that in Ref. [18] a large mixing angle is also obtained, although in the latter work [22] the authors denied this possibility.

As a short summary, based on our results of the strong decays, we find that the 2^3S_1–1^3D_1 mixing scheme with a small mixing angle $\theta_s \simeq 8.7°$ can well describe the observed $D_{s1}^*(2700)$ and $D_{s1}^*(2860)$. The weak mixing between 2^3S_1 and 1^3D_1 charm–strange mesons is also favored by Refs. [15,22–24].

3.2 1^- charm mesons

As just stated in the introduction, there are four potential 1^- resonances observed in the experiments recently, namely, $D^*(2600)$ [3], $D^*(2650)$ [5], $D_1^*(2680)$ [10] and $D_1^*(2760)$ [9]. The discrepancies among these current experimental data make the classifications more complicated than that for the corresponding charm–strange mesons. LHCb reported two 1^- states charm mesons, $D_1^*(2760)$ [9] and $D_1^*(2680)$ [10]. The two resonances have the spin–parity $J^P = 1^-$. The detected total widths are almost the same, while the mass differences are $\sim$100 MeV. Besides the two spin–parity determined 1^- states $c\bar{u}$, there are still two natural parity charm mesons $D^*(2600)$ [3] and $D^*(2650)$ [5], whose masses are located in the mass region of the 2^3S_1 state $c\bar{u}$ predicted by the GI model [11,12]. However, the measured total widths of $D^*(2600)$ and $D^*(2650)$ are inconsistent by $\sim$50 MeV.

Above all, we calculate the strong decay properties by taking all these four resonances as the 2^3S_1 or 1^3D_1 state $c\bar{u}$. The obtained results are listed in Table 5. We can see that, when taking $D^*(2600)$ as the 2^3S_1 state, both the total widths and ratio $R_{D^+}[D^*(2600)]$ are comparable with the BaBar measurements, 93 MeV and 0.32 [3]. For the other three resonances, only the total widths can be used to compare with experiments. From the calculated total widths, we can only make rough judgments, both the 2^3S_1 and 1^3D_1 assignments seem reasonable for $D^*(2650)$ and $D_1^*(2680)$, while also considering the mass predictions [11,12] they are more likely to be the 2^3S_1 states. Taking $D_1^*(2760)$ as the 1^3D_1 state $c\bar{u}$ gives the width $\sim$290 MeV, which is about 100 MeV larger than the LHCb measurement $\sim$180 MeV [9]. We also find that the decay channel $D_1^+\pi^-$ becomes quite important in the decay of the 1^3D_1 state, hence we define the ratio $R_{D_1^+} = \frac{\Gamma(D_1^+\pi^-)}{\Gamma(D^{*+}\pi^-)}$. This ratio is quite sensitive to the assignments of 2^3S_1 or 1^3D_1. All in all, for the identification

Table 4 Comparisons with other references when taking $D_{s1}^*(2700)$ and $D_{s1}^*(2860)$ as the mixtures of 2^3S_1–1^3D_1 $c\bar{s}$. Decay width Γ is in units of MeV and the mixing angle θ_s is in units of degrees

Mode	Exp.	This	Ref. [21]	Ref. [23]	Ref. [24]
θ_s	–	$8.7^{+3.9}_{-3.2}$	$-(61$–$77)$	6.8–11.2	$-(4$–$16)$
$\Gamma_{D_{s1}^*(2700)}$	117 ± 13	$100.8^{+3.1}_{-3.0}$	180–198	~ 100	$\sim(210$–$220)$
$R_K[D^*(2700)]$	0.91 ± 0.18	$0.91^{-0.18}_{+0.18}$	1.16–0.66	~ 0.91	$\sim(1.35$–$0.69)$
$\Gamma_{D_{s1}^*(2860)}$	159 ± 80	$108.8^{-1.1}_{+0.8}$	40–70	~ 300	$\sim(120$–$150)$
$R_K[D_{s1}^*(2860)]$	–	$0.62^{+0.22}_{-0.12}$	0.04–2.71	0.6–0.8	0.31–1.16

Table 5 Decay properties of $D^*(2600)$, $D^*(2650)$, $D_1^*(2680)$ and $D_1^*(2760)$ as the 2^3S_1 or 1^3D_1 dominant $c\bar{u}$ states in unit of MeV

Mode	2^3S_1				1^3D_1			
	$D^*(2600)$	$D^*(2650)$	$D_1^*(2680)$	$D_1^*(2760)$	$D^*(2600)$	$D^*(2650)$	$D_1^*(2680)$	$D_1^*(2760)$
$D^{*0}\pi^0$	12.6	15.3	17.4	25.5	2.9	3.6	4.2	5.8
$D^0\pi^0$	6.7	7.4	7.9	8.6	13.6	15.7	17.3	23.2
$D^{*+}\pi^-$	24.8	30.3	34.6	51.0	5.5	7.0	8.2	11.3
$D^+\pi^-$	13.5	15.0	16.0	17.5	26.6	30.8	34.0	46.1
$D_s^{*+}K^-$	0.1	2.1	4.8	20.0	0	0.2	0.6	2.2
$D_s^+K^-$	5.4	7.9	10.0	16.6	5.5	8.4	10.9	22.1
$D^{*0}\eta$	1.6	3.6	5.2	11.5	0.3	0.7	1.0	2.2
$D^0\eta$	3.7	4.5	5.0	5.9	5.3	6.8	7.9	12.0
$D_1^0\pi^0$	0.1	0.4	0.8	4.4	13.0	22.6	30.5	55.5
$D_1^+\pi^-$	0.1	0.6	1.4	8.3	23.6	42.9	58.6	109.1
$D_1'^0\pi^0$	0.7	0.6	0.3	0.7	0	0.002	0.005	0.04
$D_1'^+\pi^-$	1.4	1.2	0.7	1.2	0	0.004	0.008	0.07
Total	70.7	88.9	104.1	171.2	96.3	138.7	173.2	289.6
$\frac{\Gamma(D^+\pi^-)}{\Gamma(D^{*+}\pi^-)}$	0.54	0.50	0.46	0.34	4.84	4.40	4.15	4.08
$\frac{\Gamma(D_1^+\pi^-)}{\Gamma(D^{*+}\pi^-)}$	0.004	0.02	0.04	0.16	4.3	6.1	3.7	9.7

of these excited 1^- resonances, the consistent measurements from experiments are necessary and pivotal.

$D^*(2600)$ seems consistent with the 2^3S_1 assignment, while the predicted ratio $\frac{\Gamma(D^+\pi^-)}{\Gamma(D^{*+}\pi^-)} = 0.54$ is a little larger than the BaBar measurement of 0.32 [3]. This small discrepancy between theoretical and experimental results is a hint that there exists a small mixing between the 2^3S_1 and 1^3D_1 states. The physical quantity $R_{D^+}[D^*(2600)]$ can behave as a good restriction to the mixing angle, just as in the 1^- charm–strange systems. Then again we introduce the 2^3S_1–1^3D_1 mixing scheme as

$$\begin{bmatrix} |D_a^*\rangle \\ |D_b^*\rangle \end{bmatrix} = \begin{bmatrix} \cos\theta_u & \sin\theta_u \\ -\sin\theta_u & \cos\theta_u \end{bmatrix} \begin{bmatrix} |2^3S_1\rangle \\ |1^3D_1\rangle \end{bmatrix}. \tag{36}$$

At first, we take $D^*(2600)$ as the 1^- state $c\bar{u}$ dominant by 2^3S_1 components, while $D^*(2650)$ as the orthogonal partner of $D^*(2600)$. To fix the ratio $R_{D^+}[D^*(2600)]$ at BaBar's measurement $0.32^{-0.09}_{+0.09}$ [3], we obtain the mixing angle $\theta_u = -(7.5^{+4.0}_{-3.3})°$. The theoretical uncertainties are induced by varying the experimental ratio $R_{D^+}[D^*(2600)]$

in the 1σ range of its central value. Our results reveal that the mixing angle θ_u is not sensitive to the mass of D_b^*. When $m_{D_b^*}$ ranges from 2.65 to 2.78 GeV, the variation of the mixing angle is about $0.1°$. So we will ignore this tiny difference in the following statements. The partial decay widths are listed in Table 6, where $D^*(2650)$, $D^*(2680)$ or $D_1^*(2760)$ is taken as the orthogonal partner of $D^*(2600)$. The dependence of $\Gamma_{D_b^*}$ and ratio $R_{D^+}(D_b^*)$ over the mass of D_b^* can be seen in Fig. 3, where we let $m_{D_b^*}$ range from 2.65 to 2.78 GeV. It can be seen clearly in Fig. 3a that the corresponding $\Gamma_{D_b^*}$ increases from about 140–290 MeV. The predicted ratio $R_{D^+}[D_b^*]$ decreases from 9.4 to 6.8, which is displayed in Fig. 3b. The calculated total width $\Gamma_{D^*(2600)} = 66$ MeV is comparable with BaBar's measurement 93 MeV [3], while $\Gamma_{D_b^*}$ is located in the range 142–291 MeV when $m_{D_b^*}$ varies from 2.65 to 2.78 GeV.

Certainly, several other mixing schemes and corresponding assignments are still possible, however, there is no experimental ratio like $R_{D^+}[D^*(2600)]$ for $D^*(2650)$, $D_1^*(2680)$ or $D_1^*(2760)$ to restrict the mixing angle. In Table 7, the decay properties are displayed when taking $D^*(2650)$ as the

Table 6 The strong decay properties with the further 2^3S_1–1^3D_1 mixing scheme, where $D^*(2600)$ is taken as the D_a^* state and $D^*(2650)$, $D_1^*(2680)$ or $D_1^*(2760)$ is taken as the D_b^* state. The unit for decay width is in MeV. The obtained mixing angle $\theta_u = -(7.5^{+4.0}_{-3.3})°$ when the ratio $R_{D^+}[D^*(2600)]$ ranges in 1σ

Mode	$m[D_a^*]$	$m[D_b^*]$		
	2610	2650	2680	2780
$D^{*0}\pi^0$	$14.0^{+0.7}_{-0.6}$	$2.0^{-0.7}_{+0.7}$	$2.4^{-0.7}_{+0.8}$	$3.7^{-0.9}_{+0.9}$
$D^0\pi^0$	$4.4^{-1.1}_{+1.0}$	$18.1^{+1.1}_{-1.1}$	$19.7^{+1.0}_{-1.0}$	$25.3^{+0.8}_{-0.8}$
$D^{*+}\pi^-$	$27.6^{+0.2}_{-1.2}$	$3.8^{-1.3}_{+1.4}$	$4.7^{-1.5}_{+1.5}$	$7.3^{-1.9}_{+1.7}$
$D^+\pi^-$	$8.8^{-2.2}_{+2.0}$	$35.6^{+2.2}_{-2.0}$	$38.8^{+2.2}_{-2.0}$	$50.4^{+1.7}_{-2.0}$
$D_s^{*+}K^-$	0.1^{+0}_{-0}	$0.1^{-0.1}_{+0.1}$	$0.3^{-0.2}_{+0.1}$	$1.1^{-0.4}_{+0.5}$
$D_s^+K^-$	$4.0^{-0.7}_{+0.6}$	$10.3^{+1.0}_{-0.8}$	$13.3^{+1.2}_{-1.0}$	$25.6^{+1.7}_{-1.4}$
$D^{*0}\eta$	$1.8^{+0.0}_{-0.0}$	$0.3^{-0.1}_{+0.0}$	$0.5^{-0.1}_{+0.1}$	$1.2^{-0.2}_{+0.2}$
$D^0\eta$	$2.6^{-0.3}_{+0.2}$	$8.1^{+0.3}_{-0.3}$	$9.4^{+0.4}_{-0.3}$	$13.6^{+0.3}_{-0.4}$
$D_1^0\pi^0$	$0.4^{+0.4}_{-0.4}$	$22.1^{-0.6}_{+0.3}$	$29.7^{-0.7}_{+0.5}$	$54.8^{-1.1}_{+0.5}$
$D_1^+\pi^-$	$0.7^{+0.7}_{-0.3}$	$41.9^{-1.2}_{+0.6}$	$57.2^{-1.5}_{+0.8}$	$107.5^{-2.2}_{+1.1}$
$D_1'^0\pi^0$	$0.7^{-0.02}_{+0.01}$	$0.02^{+0.03}_{-0.01}$	$0.03^{+0.02}_{-0.02}$	$0.04^{+0.01}_{-0.0}$
$D_1'^+\pi^-$	$1.3^{-0.0}_{+0.1}$	$0.05^{+0.05}_{-0.03}$	$0.05^{+0.05}_{-0.03}$	$0.07^{+0.02}_{-0.01}$
Γ_{Total}	$66.4^{-2.3}_{+1.4}$	$142.4^{+0.7}_{-1.1}$	$176.1^{+0.2}_{-0.9}$	$290.6^{-2.2}_{+0.5}$
$\frac{\Gamma(D^+\pi^-)}{\Gamma(D^{*+}\pi^-)}$	$0.32^{-0.09}_{+0.09}$	$9.4^{+5.8}_{-2.9}$	$8.3^{+4.6}_{-2.3}$	$6.9^{+2.7}_{-1.5}$

$|D_a^*\rangle$ state with varying $m_{D_b^*}$ from 2.68 to 2.78 GeV, where we still assume the ratio $R_{D^+}[D^*(2650)] = 0.32 \pm 0.09$ for $D^*(2650)$. In this case, we find the mixing angle $\theta_u = -(6.1^{+4.0}_{-3.4})°$, $\Gamma_{D^*(2650)} = 85.1$ MeV and $\Gamma_{D_b^*}$ ranges in 176–292 MeV when $m_{D_b^*}$ varies from 2.68 to 2.78 GeV. Of course, we can still take $D_1^*(2680)$ as the $|D_a^*\rangle$ state and $D_1^*(2760)$ as the $|D_b^*\rangle$ state. The results should behave similarly to the above tests, the mixing angle will even be smaller, and the corresponding properties will behave almost the same as under the assignments without this further mixing.

The comparisons of our results with others can be found in Table 8, where we have also listed the properties of $D_1^*(2760)$ when taking it as the $|D_b^*\rangle$ state in order to make a comparison. From Table 8, we can see that both our small mixing angle and $\Gamma_{D^*(2600)}$ are consistent with other predictions, except for the total width in Ref. [24], which is about 3 times larger than ours. Also it should be noticed that the ratio $R_{D^+}(D_b^*)$ is sensitive to the variation of the mixing angle θ_u.

Based on our calculations and current experimental results, it is still difficult to make definite assignments to the observed $D^*(2600)$, $D^*(2650)$, $D_1^*(2680)$ or $D_1^*(2760)$. For these excited 1^- charm states, $D^{(*)}\pi$ channels are the important decay modes for both 2^3S_1 and 1^3D_1 assignments, and they can amount to (60–80) and (30–50)% of the total widths, respectively. Besides, we can still make the following summary:

1. Decay channels $D_1\pi$ become very important for 1^3D_1 state $c\bar{u}$ and can amount to about 50% among the total width, while these decay modes can be ignored in the 2^3S_1 state. This feature can be used to determined the essence of these 1^- charm resonances.
2. The properties of $D^*(2600)$ reveal that it is predominant by the 2^3S_1 component. The BaBar measured ratio $\frac{\mathcal{B}(D^+\pi^-)}{\mathcal{B}(D^{*+}\pi^-)}$ [3] can be explained by a small 2^3S_1–1^3D_1 mixing. Our obtained mixing is about $-7.5°$. This result is consistent with that for the 1^- states $D_{s1}^*(2700)$ and $D_{s1}^*(2860)$, where we got a mixing angle $\theta_s = 8.7°$.
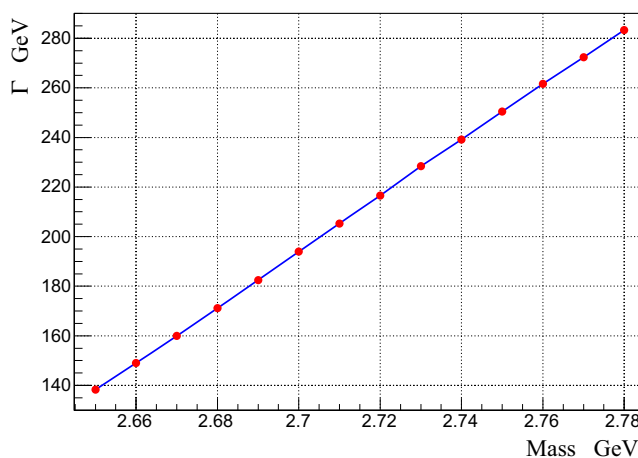
(a) Total width $\Gamma_{D_b^*}$ versus the mass.
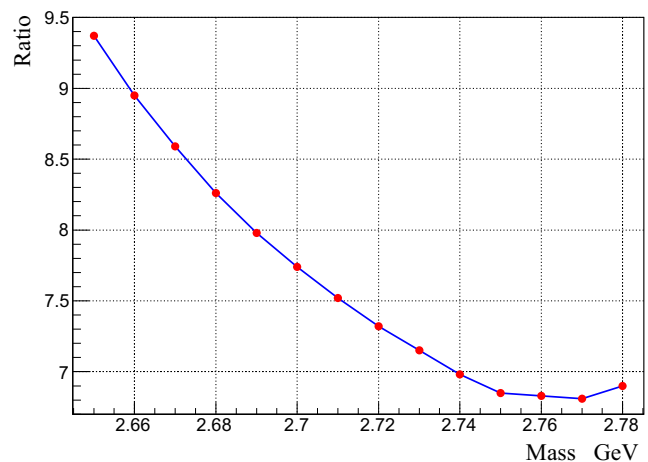
(b) $R_{D^+}(D_b^*)$ versus the mass.

Fig. 3 The variation of $\Gamma_{D_b^*}$ and the change of the ratio $R_{D^+}(D_b^*)$ along with the mass of D_b^*, where D_b^* is the state dominant by the 1^3D_1 component and $R_{D^+}(D_b^*) = \frac{\Gamma(D_b^* \to D^+\pi^-)}{\Gamma(D_b^* \to D^{*+}\pi^-)}$

Table 7 The strong decay properties with the further 2^3S_1–1^3D_1 mixing scheme, where $D^*(2650)$ is taken as the D_a^* state and the mass of D_b^* is taken as 2.68, 2.73 and 2.78 GeV, respectively. We assume that the ratio $\frac{\mathcal{B}(D^+\pi^-)}{\mathcal{B}(D^{*+}\pi^-)} = 0.32 \pm 0.09$, as for $D^*(2600)$. Our obtained mixing angle $\theta_u = -(6.1^{+4.0}_{-3.4})°$. The unit for the decay width is MeV

Mode	$m[D_a^*]$	$m[D_b^*]$		
	2650	2680	2730	2780
$D^{*0}\pi^0$	$16.7^{+0.8}_{-0.7}$	$2.6^{-0.8}_{+0.9}$	$3.4^{-1.0}_{+1.0}$	$3.9^{-1.0}_{+1.0}$
$D^0\pi^0$	$5.2^{-1.3}_{+1.2}$	$19.5^{+1.2}_{-1.2}$	$22.2^{+1.2}_{-1.2}$	$25.3^{+1.1}_{-1.1}$
$D^{*+}\pi^-$	$33^{+1.6}_{-1.4}$	$5.1^{-1.7}_{+1.7}$	$6.6^{-2.0}_{+1.9}$	$7.7^{-2.1}_{+1.9}$
$D^+\pi^-$	$10.6^{-2.7}_{+2.3}$	$38.4^{+2.6}_{-2.3}$	$44^{+2.5}_{-2.3}$	$50.3^{+2.3}_{-2.2}$
$D_s^{*+}K^-$	$2.2^{+0.03}_{-0.09}$	$0.3^{-0.2}_{+0.1}$	$0.7^{-0.3}_{+0.4}$	$1.2^{-0.5}_{+0.5}$
$D_s^+K^-$	$6.2^{-1.1}_{+1.0}$	$13^{+1.4}_{-1.1}$	$18.6^{+1.6}_{-1.5}$	$25.4^{+1.9}_{-1.8}$
$D^{*0}\eta$	$3.9^{+0.1}_{-0.2}$	$0.6^{-0.2}_{+0.2}$	$1^{-0.3}_{-0.4}$	$1.4^{-0.5}_{+0.4}$
$D^0\eta$	$3.3^{-0.7}_{+0.7}$	$9.2^{+0.8}_{-0.7}$	$11.3^{+0.8}_{-0.8}$	$13.5^{+0.8}_{-0.8}$
$D_1^0\pi^0$	$0.8^{+0.5}_{-0.3}$	$29.9^{-0.7}_{+0.4}$	$43^{-0.9}_{+0.4}$	$55^{-1.0}_{+0.4}$
$D_1^+\pi^-$	$1.4^{+1.0}_{-0.5}$	$57.6^{-1.4}_{+0.7}$	$83.7^{-1.8}_{+0.9}$	$107.9^{-2.0}_{+0.9}$
$D_1'^0\pi^0$	$0.6^{-0.02}_{-0.0}$	$0.01^{+0.02}_{-0.0}$	$0.02^{+0.01}_{-0.0}$	$0.04^{-0.04}_{-0.0}$
$D_1'^+\pi^-$	$1.2^{+0.0}_{-0.0}$	$0.03^{+0.03}_{-0.02}$	$0.04^{+0.02}_{-0.01}$	$0.06^{+0.05}_{+0.01}$
Γ_{Total}	$85.1^{-1.7}_{+1.9}$	$176.2^{+1.0}_{-1.4}$	$234.6^{-0.2}_{-0.9}$	$291.7^{-0.8}_{-0.8}$
$\frac{\Gamma(D^+\pi^-)}{\Gamma(D^{*+}\pi^-)}$	$0.32^{-0.09}_{+0.09}$	$7.53^{+4.56}_{-2.19}$	$6.67^{+3.28}_{-1.76}$	$6.53^{+2.89}_{-1.52}$

3. The mass of $D_1^*(2760)$ is consistent with the prediction of the 1^3D_1 state $c\bar{u}$ [11,12]. If we take this assignment, the measured total width seems too small (the LHCb result [9] is about 100 MeV smaller than the theoretical calculation). This conclusion is also favored by the research in Refs. [12,21,24,27,33].

4. $D^*(2650)$ is more likely to be the 2^3S_1 predominant state. There is no great conflict in the total widths of the 2^3S_1 and 1^3D_1 assignments, while its mass is more consistent with the 2^3S_1 state. The ratio $\frac{\Gamma(D^+\pi^-)}{\Gamma(D^{*+}\pi^-)}$ behaves quite differently for the two assignments, which is 0.5 for the 2^3S_1 assignment and 4.4 for the 1^3D_1 assignment. Hence this ratio can be used to test the essence of $D^*(2650)$.

5. For $D_1^*(2680)$, the situation is similar to $D^*(2650)$. There exists no great conflict in the total widths between the

2^3S_1 and 1^3D_1 assignments compared with experimental measurements. The ratios $\frac{\Gamma(D^+\pi^-)}{\Gamma(D^{*+}\pi^-)}$ are 0.46 and 4.15 for the 2^3S_1 and 1^3D_1 assignments, respectively; therefore they can be used to discern the essence of $D_1^*(2680)$.

4 Summary

In this work, we carried out a systematical research on the potential 1^- open charm mesons, including the charm–strange mesons $D_{s1}^*(2700)$ and $D_{s1}^*(2860)$, charm mesons $D^*(2600)$, $D^*(2650)$, $D_1^*(2680)$ and $D_1^*(2760)$. The main strong decay properties by taking these natural spin–parity resonances as the 2^3S_1 or 1^3D_1 states are obtained by using the Bethe–Salpeter method. In particularly, the further $2S$–$1D$ mixing scheme is used to explain both the 1^- charm and charm–strange mesons. The obtained results and predicted properties can be tested in the near future experiments.

Our results reveal that $D_{s1}^*(2700)$ and $D_{s1}^*(2860)$ can be well described by the further 2^3S_1–1^3D_1 mixing scheme with a small mixing angle $(8.7^{+3.9}_{-3.2})°$. Both the total widths and the ratio of the corresponding partial decay widths are consistent with the experimental measurements. Our predicted ratio $\frac{\Gamma(D^*K)}{\Gamma(DK)}$ for $D_{s1}^*(2860)$ is $0.62^{+0.22}_{-0.12}$, which could be used to test this $2S$–$1D$ mixing scheme in the future. For the corresponding charm mesons, since the experimental measurements are not consistent with each other, the identification and assignments are much more difficult. Based on our results, the BaBar result for $D^*(2600)$ [3] can be explained by the same mixing scheme with a mixing angle of $-(7.5^{+4.0}_{-3.3})°$. $D^*(2650)$ [5] and $D_1^*(2680)$ [10] are more likely 2^3S_1 predominant states, since their masses are consistent with the 2^3S_1 predictions, while our calculated total widths are both comparable with the experimental measurements under the 2^3S_1 or 1^3D_1 assignments. Our results also show that the measured width of $D_1^*(2760)$ is much smaller than the theoretical calculations under the 1^3D_1 assignment. This would be an obstacle to identifying $D_1^*(2760)$ as the 1^3D_1 predominant $c\bar{u}$. There still exist puzzles and difficulties in the identifications of these new excited charmed mesons. Further precise

Table 8 Comparison with other references when taking $D^*(2600)$ as the mixture of 2^3S_1–1^3D_1 $c\bar{u}$. Γ_{Tot} is in units of MeV and the mixing angle θ_u is in units of degree

$D^*(2600)$	Exp.	This	Ref. [21]	Ref. [27]	Ref. [24]	Ref. [33]
θ_u	–	$-(7.5^{+4.0}_{-3.3})$	$-(21\text{–}23)$	$-(36\pm6)$	$(4\text{–}17)$	$(-3.6\text{–}1.8)$
$\Gamma_{D^*(2600)}$	93 ± 14.3	$66.4^{-2.3}_{+1.4}$	74–80	75–115	205–195	∼60
$R_{D^+}[D^*(2600)]$	0.32 ± 0.09	$0.32^{-0.09}_{+0.09}$	0.38–0.43	0.63 ± 0.21	∼(0.25–0.53)	∼0.32
$\Gamma_{D_1^*(2760)}$	177 ± 38.4	$290.6^{-2.2}_{+0.5}$	280–310	300–550	∼290	385
$R_{D^+}[D_1^*(2760)]$	–	$6.9^{+2.7}_{-1.5}$	1.25–2.25	–	(2.62–28.86)	2.2

measurements of their properties are needed and are important.

References

1. J. Brodzicka et al., Belle Collaboration, Phys. Rev. Lett. **100**, 092001 (2008). doi:10.1103/PhysRevLett.100.092001
2. B. Aubert et al., BaBar Collaboration, Phys. Rev. D **80**, 092003 (2009). doi:10.1103/PhysRevD.80.092003
3. P. del Amo Sanchez et al., BaBar Collaboration, Phys. Rev. D **82**, 111101(R) (2010). doi:10.1103/PhysRevD.82.111101
4. R. Aaij et al. (LHCb Collaboration), J. High Energ. Phys. **2012**, 151 (2012). doi:10.1007/JHEP10(2012)151
5. R. Aaij et al. (LHCb Collaboration), J. High Energ. Phys. **2013**, 145 (2013). doi:10.1007/JHEP09(2013)145
6. R. Aaij et al., LHCb Collaboration, Phys. Rev. Lett **113**, 162001 (2014). doi:10.1103/PhysRevLett.113.162001
7. K. Olive et al., Particle Data Group, Chin. Phys. C **38**, 090001 (2014). doi:10.1088/1674-1137/38/9/090001
8. J.P. Lees et al., BaBar Collaboration, Phys. Rev. D **91**, 052002 (2015). doi:10.1103/PhysRevD.91.052002
9. R. Aaij et al., LHCb Collaboration, Phys. Rev. D **91**, 092002 (2015). doi:10.1103/PhysRevD.91.092002
10. R. Aaij et al., LHCb Collaboration, Phys. Rev. D **94**, 072001 (2016). doi:10.1103/PhysRevD.94.072001
11. S. Godfrey, N. Isgur, Phys. Rev. D **32**, 189 (1985). doi:10.1103/PhysRevD.32.189
12. S. Godfrey, K. Moats, Phys. Rev. D **93**, 034035 (2016). doi:10.1103/PhysRevD.93.034035
13. P. Colangelo, F. De Fazio, S. Nicotri, M. Rizzi, Phys. Rev. D **77**, 014012 (2008). doi:10.1103/PhysRevD.77.014012
14. B. Chen, D.-X. Wang, A. Zhang, Phys. Rev. D **80**, 071502(R) (2009). doi:10.1103/PhysRevD.80.071502
15. B. Chen, L. Yuan, A. Zhang, Phys. Rev. D **83**, 114025 (2011). doi:10.1103/PhysRevD.83.114025
16. A. Zhang, Nucl. Phys. A **856**, 88–94 (2011). doi:10.1016/j.nuclphysa.2011.02.004
17. J. Segovia, D.R. Entem, F. Fernandez, Phys. Rev. D **91**, 094020 (2015). doi:10.1103/PhysRevD.91.094020
18. S. Godfrey, I.T. Jardine, Phys. Rev. D **89**, 074023 (2014). doi:10.1103/PhysRevD.89.074023
19. X.-H. Zhong, Q. Zhao, Phys. Rev. D **81**, 014031 (2010). doi:10.1103/PhysRevD.81.014031
20. D.-M. Li, B. Ma, Phys. Rev. D **81**, 014021 (2010). doi:10.1103/PhysRevD.81.014021
21. D.-M. Li, P.-F. Ji, B. Ma, Eur. Phys. J. C **71**, 1582 (2011). doi:10.1140/epjc/s10052-011-1582-9
22. S. Godfrey, K. Moats, Phys. Rev. D **90**, 117501 (2014). doi:10.1103/PhysRevD.90.117501
23. Q.-T. Song, D.-Y. Chen, X. Liu, T. Matsuki, Phys. Rev. D **91**, 054031 (2015). doi:10.1103/PhysRevD.91.054031
24. B. Chen, X. Liu, A. Zhang, Phys. Rev. D **92**, 034005 (2015). doi:10.1103/PhysRevD.92.034005
25. F.-K. Guo, U.-G. Meibner, Phys. Rev. D **84**, 014013 (2011). doi:10.1103/PhysRevD.84.014013
26. T. Wang, Z.-H. Wang, Y. Jiang, L. Jiang, G.-L. Wang, Eur. Phys. J. C **77**, 38 (2017)
27. X.-H. Zhong, Phys. Rev. D **82**, 114014 (2010). doi:10.1103/PhysRevD.82.114014
28. Z.-G. Wang, Phys. Rev. D **83**, 014009 (2011). doi:10.1103/PhysRevD.83.014009
29. Z.-G. Wang, Phys. Rev. D **88**, 114003 (2013). doi:10.1103/PhysRevD.88.114003
30. P. Colangelo, F. De Fazio, F. Giannuzzi, S. Nicotri, Phys. Rev. D **86**, 054024 (2012). doi:10.1103/PhysRevD.86.054024
31. Z.-F. Sun, J.-S. Yu, X. Liu, Phys. Rev. D **82**, 111501(R) (2010). doi:10.1103/PhysRevD.82.111501
32. Q.-F. Lü, D.-M. Li, Phys. Rev. D **90**, 054024 (2014). doi:10.1103/PhysRevD.90.054024
33. Q.-T. Song, D.-Y. Chen, X. Liu, T. Matsuki, Phys. Rev. D **92**, 074011 (2015). doi:10.1103/PhysRevD.92.074011
34. G.-L. Yu, Z.-G. Wang, Z.-Y. Li, Phys. Rev. D **94**, 074024 (2016). doi:10.1103/PhysRevD.94.074024
35. J.L. Rosner, Commun. Nucl. Part. Phys. **16**(3), 109 (1986)
36. S. Godfrey, R. Kokoski, Phys. Rev. D **43**, 1679 (1991). doi:10.1103/PhysRevD.43.1679
37. J.L. Rosner, Ann. Phys. **319**(1), 1 (2005). doi:10.1016/j.aop.2005.02.004
38. G.-L. Wang, Y. Jiang, T. Wang, W.-L. Ju, arXiv:1305.4756 [hep-ph]
39. E.E. Salpeter, H. Bethe, Phys. Rev. **84**, 1232 (1951). doi:10.1103/PhysRev.84.1232
40. E.E. Salpeter, Phys. Rev. **87**, 328 (1952). doi:10.1103/PhysRev.87.328
41. C.-H. Chang, C.S. Kim, G.-L. Wang, Phys. Lett. B **623**, 218 (2005). doi:10.1016/j.physletb.2005.07.059
42. Z.-H. Wang, G.-L. Wang, H.-F. Fu, Y. Jiang, Phys. Lett. B **706**, 389 (2012). doi:10.1016/j.physletb.2011.11.051
43. T. Wang, G.-L. Wang, H.-F. Fu, W.-L. Ju, JHEP **07**, 120 (2013). doi:10.1007/JHEP07(2013)120
44. Z.-H. Wang, Y. Zhang, L.-B. Jiang, T.-H. Wang, Y. Jiang, G.-L. Wang, Eur. Phys. J. C **77**, 43 (2017). doi:10.1140/epjc/s10052-017-4596-0
45. W.-L. Ju, G.-L. Wang, H.-F. Fu, Z.-H. Wang, Y. Li, JHEP **09**, 171 (2015). doi:10.1007/JHEP09(2015)171
46. Q. Li, T. Wang, Y. Jiang, H. Yuan, G.-L. Wang, Eur. Phys. J. C **76**, 454 (2016). doi:10.1140/epjc/s10052-016-4306-3
47. Q. Li, T. Wang, Y. Jiang, H. Yuan, T. Zhou, G.-L. Wang, Eur. Phys. J. C **77**, 12 (2017). doi:10.1140/epjc/s10052-016-4588-5
48. G.-L. Wang, Phys. Lett. B **633**, 492 (2006). doi:10.1016/j.physletb.2005.12.005
49. G.-L. Wang, Phys. Lett. B **674**, 172 (2009). doi:10.1016/j.physletb.2009.03.030
50. T. Wang, G.-L. Wang, W.-L. Ju, Y. Jiang, JHEP **03**, 110 (2013). doi:10.1007/JHEP03(2013)110
51. V.B. Berestetskii, E.M. Lifshitz, L.P. Pitaevskii, Quantum Electrodynamics, 2nd edn, no 83 (1982)
52. S. Mandelstam, Proc. R. Soc. A **233**, 248 (1955). doi:10.1098/rspa.1955.0261
53. C.S. Kim, G.-L. Wang, Phys. Lett. B **584**, 285 (2004). doi:10.1016/j.physletb.2004.01.058
54. T. Wang, G.-L. Wang, Y. Jiang, W.-L. Ju, J. Phys. G. **40**, 035003 (2013). doi:10.1088/0954-3899/40/3/035003
55. T. Wang, H.-F. Fu, Y. Jiang, Q. Li, G.-L. Wang, Int. J. Mod. Phys. A **32**, 1750035 (2017)

56. C.-H. Chang, J.-K. Chen, X.-Q. Li, G.-L. Wang, Commun. Theor. Phys. **43**, 113 (2005). http://stacks.iop.org/0253-6102/43/i=1/a=023
57. C.-H. Chang, G.-L. Wang, Sci. China. Phys. Mech. Astron. **53**, 2005 (2010). doi:10.1007/s11433-010-4156-1
58. T. Matsuki, T. Morii, K. Seo, Prog. Theor. Phys. **124**, 2 (2010). doi:10.1143/PTP.124.285
59. D. Ebert, R.N. Faustov, V.O. Galkin, Eur. Phys. J. C **66**, 197 (2010). doi:10.1140/epjc/s10052-010-1233-6
60. G.-L. Wang, Phys. Lett. B **650**, 15 (2007). doi:10.1016/j.physletb.2007.05.001
61. C.-H. Chang, G.-L. Wang, Sci. China Phys. Mech. Astron. **53**, 2005 (2010). doi:10.1007/s11433-010-4156-1
62. H.-F. Fu, Y. Jiang, C.S. Kim, G.-L. Wang, JHEP **06**, 015 (2011). doi:10.1007/JHEP06(2011)015
63. Z.-H. Wang, G.-L. Wang, H.-F. Fu, Y. Jiang, Phys. Lett. B **706**, 389 (2012)
64. Z.-H. Wang, G.-L. Wang, H.-F. Fu, Y. Jiang, Int. J. Mod. Phys. A **27**, 1250049 (2012)
65. S.-C. Li, Y. Jiang, T.-H. Wang, Q. Li, Z.-H. Wang, G.-L. Wang, Mod. Phys. Lett. A **32**, 1750013 (2017)
66. S.-C. Zhang, T.-H. Wang, Y. Jiang, Q. Li, G.-L. Wang, Int. J. Mod. Phys. A **32**, 1750022 (2017)
67. G. Ecker, J. Gasser, A. Pich, E. de Rafael, Nucl. Phys. B **321**, 311–342 (1989)